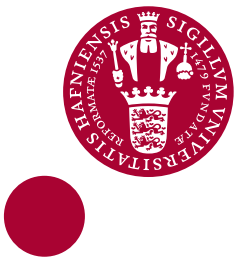

Synthesis, Radiolabeling, and in Vitro and in Vivo Evaluation of [18F]ENL30

A Potential PET Radiotracer for the 5-HT7 Receptor

Tampio L'Estrade, Elina; Edgar, Fraser G.; Xiong, Mengfei; Shalgunov, Vladimir; Baerentzen, Simone L.; Erlandsson, Maria; Ohlsson, Tomas G.; Palner, Mikael; Knudsen, Gitte M.; Herth, Matthias M.

Published in:
ACS Omega

DOI:
10.1021/acsomega.9b00394

Publication date:
2019

Document version
Publisher's PDF, also known as Version of record

ACS OMEGA

Article

Cite This: ACS Omega 2019, 4, 7344−7353

http://pubs.acs.org/journal/acsodf

Synthesis, Radiolabeling, and in Vitro and in Vivo Evaluation of [^{18}F]ENL30: A Potential PET Radiotracer for the 5-HT$_7$ Receptor

Elina Tampio L'Estrade,[†,‡,§] Fraser G. Edgar,[‡] Mengfei Xiong,[†,‡] Vladimir Shalgunov,[‡] Simone L. Baerentzen,[†] Maria Erlandsson,[§] Tomas G. Ohlsson,[§] Mikael Palner,[†,∥] Gitte M. Knudsen,[†,⊥] and Matthias M. Herth*[,‡,#]

[†]Neurobiology Research Unit, Rigshospitalet, Blegdamsvej 9, 2100 Copenhagen, Denmark

[‡]Department of Drug Design and Pharmacology, Faculty of Health and Medical Sciences, University of Copenhagen, Jagtvej 160, 2100 Copenhagen, Denmark

[§]Radiation Physics, Nuclear Medicine Physics Unit, Skånes University Hospital, Barngatan 3, 222 42 Lund, Sweden

[∥]Center for Translational Neuromedicine, University of Copenhagen, Blegdamsvej 3B, 2200 Copenhagen N, Denmark

[⊥]Faculty of Health and Medical Sciences, University of Copenhagen, 2200 Copenhagen, Denmark

[#]Department of Clinical Physiology, Nuclear Medicine and PET, University Hospital Copenhagen, Rigshospitalet Blegdamsvej 9, 2100 Copenhagen, Denmark

Supporting Information

ABSTRACT: The 5-HT$_7$ receptor (5-HT$_7$R) is involved in a broad range of physiological conditions and disorders. Currently, there is no validated clinical positron emission tomography (PET) tracer available; however, we have recently developed a promising ^{11}C-labeled candidate. In this project, we aimed to further extend our efforts and develop an ^{18}F-labeled derivative, coined [^{18}F]ENL30. Fluorine-18 has several advantages over carbon-11 especially within the preclinical phase, where a long half-life usually increases evaluation throughput. ENL30 was successfully synthesized in a low albeit sufficient overall yield. Radiolabeling succeeded with a radiochemical yield of approximately 4.5%. Subsequent preclinical PET studies revealed that [^{18}F]ENL30 binds specifically to the 5-HT$_7$R but suffered from affinity to σ-receptors. Additionally, we identified [^{18}F]ENL30 to be a *P*-gp substrate in rats. However, we believe that [^{18}F]ENL30 may prove to be valuable in higher species that exhibit decreased *P*-gp dependency. If required, σ-receptor binding could, in such studies, be selectively blocked potentially allowing for selective 5-HT$_7$R imaging.

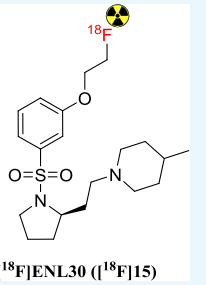

[^{18}F]ENL30 ([^{18}F]15)

INTRODUCTION

The serotonergic system with its neurotransmitter serotonin (5-hydroxytryptamine, 5-HT) is widely spread throughout the brain and modulates a variety of psychological and behavioral functions and disorders.[1,2] In 1993, the 5-HT$_7$ receptor (5-HT$_7$R) was identified and became the most recent member to be added to the serotonin receptor family.[3−5] The 5-HT$_7$R is a G-protein-coupled receptor, positively coupled to adenylate cyclase, with activation leading to the production of cyclic adenosine monophosphate, which in turn is involved in a broad spectrum of secondary cell activation pathways.[2−5] The 5-HT$_7$R is abundant in the central nervous system (CNS) with the highest concentrations in thalamus (tha), hypothalamus, hippocampus, and cortex (see Table S1, Supporting Information, for further details).[6−10] Preclinical studies with, e.g., 5-HT$_7$R knockout mice, have associated this receptor with CNS disorders such as depression, anxiety, and schizophrenia.[1,11−16] Currently, there is no clinical imaging radiotracer available to study the 5-HT$_7$R in vivo.[1,17] Access to such a radiotracer would enable the study of the receptor's physiological function and its involvement in various CNS diseases. Furthermore, since the 5-HT$_7$R displays the highest affinity toward serotonin of all serotonergic receptors, 5-HT$_7$R neuroimaging could be a valuable tool in determining changes in the concentration of 5-HT in the synaptic cleft.[18] This could significantly improve our understanding of the involvement of endogenous 5-HT in brain disorders[19] and potentially provide a path for new treatment options.

Positron emission tomography (PET) is a nuclear medicine molecular imaging technique that can be used to visualize and quantify receptor physiology in vivo.[20−22] Consequently, a PET tracer for the 5-HT$_7$R would allow the study of this receptor system in vivo and address the aforementioned research questions. Several groups, including ours, have over the years attempted to develop a 5-HT$_7$R radiotracer, although so far with limited success.[9,23−29] For example, PET tracers evaluated in pigs or cats with promising outcomes, such as [^{18}F]2FP3 or [^{11}C]Cimbi-717 (Figure 1), did not produce a specific signal in nonhuman primates.[10,30] Other tracers failed at even earlier evaluation stages.[26,28,29]

Received: February 12, 2019
Accepted: April 12, 2019
Published: April 23, 2019

DOI: 10.1021/acsomega.9b00394
ACS Omega 2019, 4, 7344−7353

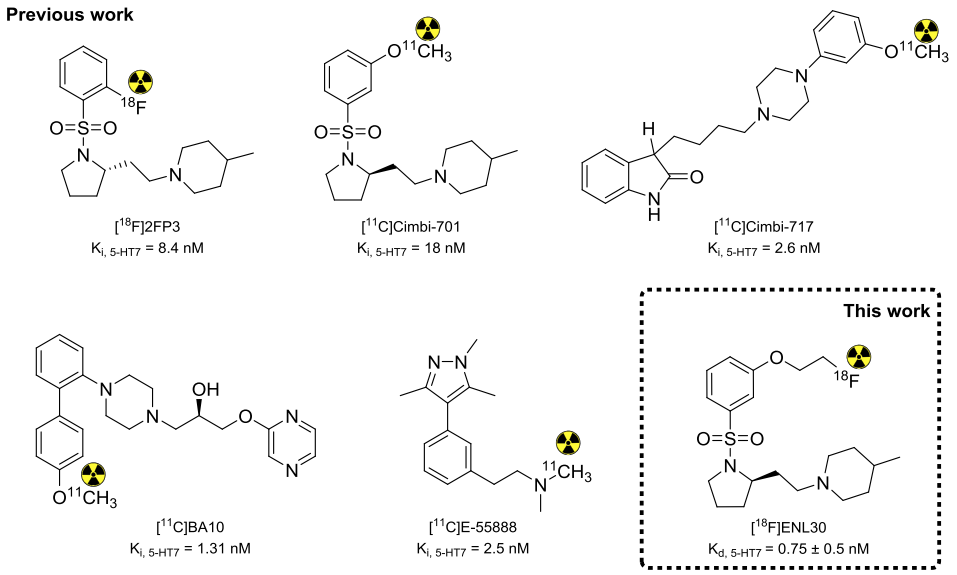

Figure 1. Schematic overview of previously evaluated PET tracers for the 5-HT$_7$R and the structure of the new potential PET tracer presented in this work, [^{18}F]ENL30.[9,10,25,26,28,31]

Scheme 1. Synthetic Overview of ENL30 (15)[a]

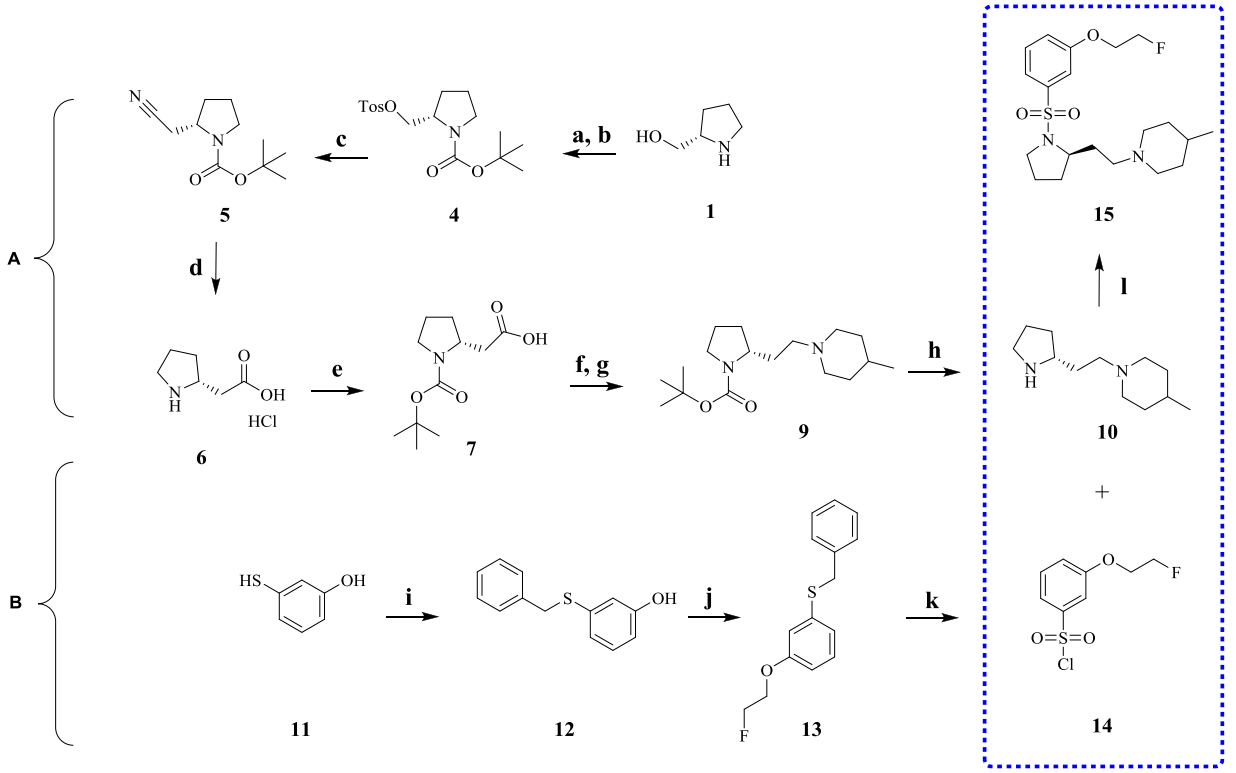

[a](A) The synthesis of (*R*)-4-methyl-1-(2-(pyrrolidin-2-yl)ethyl)piperidine (**10**), (B) its sulfonyl chloride coupling partner (**14**) and the final coupling to form the sulfonamide product **15** (right). Reagents and conditions: (a) $(Boc)_2O$, triethylamine (TEA), MeOH, Δ, 0.5 h; (b) *p*-TosCl, Py, dichloromethane (DCM), 0 °C—room temperature (rt), overnight; (c) potassium cyanide (KCN), dimethyl sulfoxide (DMSO), 90 °C, 4 h; (d) HCl (35%), AcOH, Δ, 6 h; (e) $(Boc)_2O$, NaOH (2 M), acetone, 0 °C—rt, 2.5 h; (f) borane−tetrahydrofuran (THF), THF, rt, ON; (g) (i) MsCl, Py, DCM, 0 °C—rt, 2 h; (ii) 4-methylpiperidine, acetonitrile (ACN), rt—50 °C, ON; (h) trifluoroacetic acid (TFA)/DCM (1:1), rt, 0.5 h. (i) BnBr, NaOH, MeOH, H_2O, AcOH, ON; (j) 1-bromo-2-fluoroethane, NaH, dimethylformamide (DMF), 0−60 °C, 20 h; (k) 1,3-dichloro-5,5-dimethylhydantoin, ACN, AcOH, H_2O, 0 °C, 5 h. (l) Et_2O, NaOH, 0 °C—rt, ON.

Our group has recently developed an O-methylated carbon-11-labeled derivative of the highly selective 5-HT$_7$R antagonist SB-269970 (Figure 1).[31] This tracer ([^{11}C]Cimbi-701) has shown promising results in pigs,[30] prompting us to extend this work and develop an ^{18}F-labeled analogue. Fluorine-18 has several advantages over carbon-11 in respect to clinical translation and also preclinical work in rodents. Namely, the use of fluorine-18 can result in higher spatial resolution.

DOI: 10.1021/acsomega.9b00394
ACS Omega 2019, 4, 7344−7353

Moreover, the longer half-life of fluorine-18 (109 vs 20.4 min) eases the use for multiple evaluation experiments with a single production.[21]

RESULTS AND DISCUSSION

A common strategy to convert a carbon-11 tracer into a fluorine-18 analogue is to exchange a methoxy functional group for a fluoroethoxy moiety. [^{18}F]MH.MZ is one of the many examples where this strategy has been successfully applied.[32−34] This attractive approach is not thought to drastically impact the pharmacological behavior of the tracer due to similar electronic, inductive, and spatial properties of the two moieties.[34] In light of that, we were inspired to apply this approach to [^{11}C]Cimbi-701 and develop an ^{18}F-labeled derivative ([^{18}F]ENL30). The reference compound ENL30 (**15**) was synthesized in a way similar to a previously reported synthesis strategy that was applied to a phenolic analogue (Scheme 1).[31,35,36]

A key intermediate for this synthesis route is (*R*)-4-methyl-1-(2-(pyrrolidin-2-yl)ethyl)piperidine (**10**), which we initially tried to synthesize with a procedure described by Lovell et al.[31] However, the necessary intermediate *tert*-butyl-2-(((methylsulfonyl)oxy)methyl)pyrrolidine-1-carboxylate (**3**) and its subsequent transformation suffered from poor yields (Tables 1 and 2). As such, other leaving groups and reaction conditions were employed. The use of tosyl chloride and pyridine in DCM resulted in sufficient yields of the tosylate (**4**), which could then be satisfactorily transformed to the nitrile (**5**) in DMSO. This led to an optimized and satisfying yield of approximately 63% over those two steps (Tables 1 and 2).[31,35,36]

Several catalyst-mediated reaction routes have been reported to form (**10**) directly from (**5**).[31,37] However, in our hands, even extensive optimization efforts did not result in any satisfying yields (see the Supporting Information for more details). It appeared that although the initial hydrogenation did occur (nitrile to imide) the catalyst failed to eliminate the ammonia in the final step. In light of that, a previously described multistep route was chosen to synthesize (**10**) (Scheme 1). This strategy was initially thought to be inferior since an unnecessary deprotection/protection had to be applied. However, this approach yielded in sufficient amounts of (**10**) that could be used in a subsequent coupling step with another key intermediate 3-(2-fluoroethoxy)benzenesulfonyl chloride (**14**).[31,35,36,38] The synthesis of (**14**) is detailed in Scheme 1. Notably, in the final step in the synthesis of **14**, the need for *S*-deprotection was circumvented and allowed direct oxidation of sulfur.[39,40] In summary, the reference synthesis was completed in 13 steps, ending up with an overall low yield of approximately 0.2%.

In the next step, radiolabeling of [^{18}F]ENL30 ([^{18}F]**15**) was attempted applying a two-step labeling procedure starting from the commercially available precursor SB-269970 (3-[[(2R)-2-[2-(4-methyl-1-piperidinyl)ethyl]-1-pyrrolidinyl]sulfonyl]-phenol, monohydrochloride) and the routinely produced synthon, 2-[^{18}F]fluoroethyl tosylate ([^{18}F]FETos). Using this strategy, [^{18}F]**15** could successfully be radiolabeled in a radiochemical yield (RCY) ranging between 1.2 and 15% (decay corrected, n = 8), with satisfactory molar activities [108−197 GBq/μmol (n = 3)] and radiochemical purities of >98% (Scheme 2). The total synthesis time including separation and formulation took less than 180 min. A maximum amount of 0.9 GBq was isolated using this approach. Importantly, it was necessary to form the phenolate before starting the labeling procedure. Adding the base 40 min prior to initiating the reaction at 100 °C resulted in the highest RCY.

Encouraged by these results, we performed autoradiographic studies on coronal rat brain slices, containing thalamus, a high 5-HT$_7$R density region (Figure 2a−c).[6−10] These studies were conducted to determine the affinity and selectivity of [^{18}F]**15** toward the 5-HT$_7$R. A K_D of 0.75 ± 0.5 nM (n = 9) for the 5-HT$_7$R could be determined in a saturation assay (Figure 2d). Recently, a close analogues of [^{18}F]**15** displayed affinity toward σ-receptors when subjected to competition assays, so we decided to evaluate the selectivity of [^{18}F]**15** toward these receptors by performing autoradiographic blocking studies with the 5-HT$_7$R selective antagonist SB-269970 ($K_{i,5\text{-HT}_7}$ = 1.26 nM, $K_{i,5\text{-HT5a}}$ = 32 nM, and $K_{i,\sigma-1}$ = 158 nM)[31,41] as well as with haloperidol as a σ-receptor-blocking agent ($K_{i,D2}$ = 2 nM, $K_{i,D3}$ = 4 nM, $K_{i,\sigma-1}$ = 4 nM, $K_{i,\alpha1}$ = 12 nM, $K_{i,\sigma-2}$ = 14 nM, $K_{i,D4}$ = 15 nM, $K_{i,5\text{-HT}_2A}$ = 70 nM, and $K_{i,5\text{-HT}_7}$ = 380 nM).[42−44] The results are displayed in Figure 2e. We found a dose-dependent blocking with both ligands, 13% blockage using a 50 nM solution of SB-269970 and 10.5% blockage using a 50 nM solution of

Table 1. Incorporation of a Suitable Leaving Group

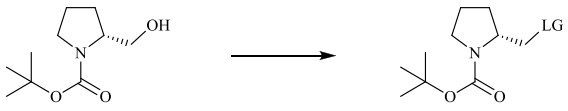

2 **3 or 4**

leaving group (LG)	solvent	base	temperature (°C)	time (h)	yield (%)
OMs	THF	TEA	−78—rt	2	12.6
OTos	DCM	TEA, cat. DMAP	rt	6	28.6
OTos	DCM	pyridine	0—rt	overnight	76.8

Table 2. Optimization of Nitrile Introduction

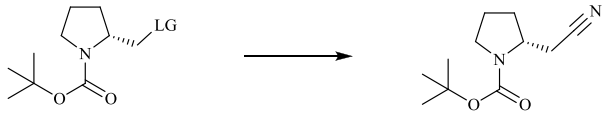

3 or 4 **5**

leaving group (LG)	solvent	temperature (°C)	time (h)	XCN	yield (%)
OMs	DMF	100	6	NaCN	33.4
OMs	EtOH	reflux	overnight	KCN	N/A
OTos	DMSO	90	4	KCN	81.9

Scheme 2. Radiosynthesis of [^{18}F]ENL30 ([^{18}F]15) (a) [^{18}F]F$^-$, K_{222}, K_2CO_3, ACN, 80 °C, 3 min; (b) DMF, NaOH (2N), 100 °C, 25 min

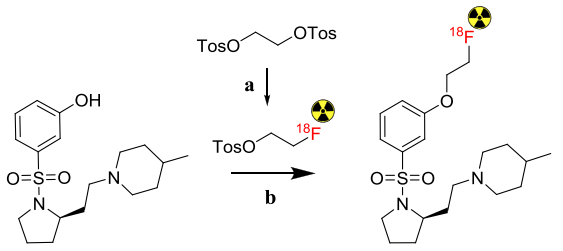

SB-269970 **[^{18}F]ENL30 ([^{18}F]15)**

DOI: 10.1021/acsomega.9b00394
ACS Omega 2019, 4, 7344−7353

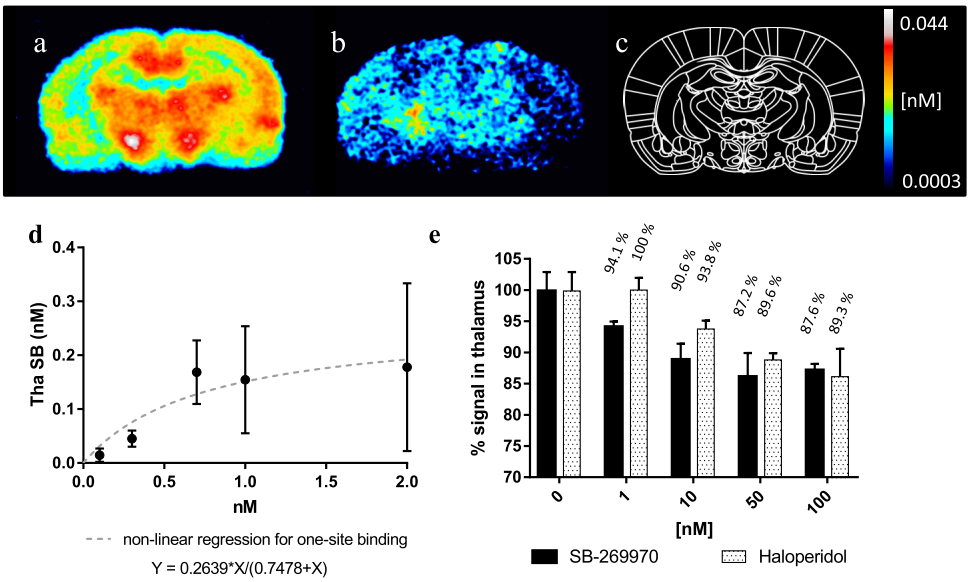

Figure 2. Results of the in vitro evaluation of [^{18}F]**15**. (a–d) Determination of K_D and B_{max} values of [^{18}F]**15** in the thalamus (Tha). (a) Coronal rat brain slice displaying the total binding of [^{18}F]**15**. (b) Coronal rat brain slice displaying the nonspecific binding of [^{18}F]**15** by blocking with SB-269970 (10 μm). (c) Location of brain slices, around bregma −1.8. (d) K_D and B_{max} were elucidated from one-sited (specific binding, SB) nonlinear regression plotting the specific binding (SB) in nM of [^{18}F]**15** tracer concentration in nM. The data is based on five concentrations (0.1, 0.3, 0.7, 1, and 2 nM) and experiments were repeated three times (n = 9). (e) In vitro autoradiography blocking study. The results are shown as a grouped barplot with the % signal in thalamus compared to 0 nM (total binding) using different concentrations (1, 10, 50, and 100 nM) of SB-269970 and haloperidol (n = 3). Error bars represent standard deviation (SD).

haloperidol. Consequently, [^{18}F]**15**, in addition to 5-HT$_7$R binding, also binds to σ-receptors.

Specific and selective PET imaging is dependent on three key factors: (1) affinity ($1/K_D$), (2) regional target density (B_{max}) compared to the density of other off-targets, and (3) nonspecific binding.[19,22,45] In vivo nonspecific binding is usually only not determinable in vitro, even though more lipophilic tracers tend to have higher nonspecific binding.[22,46] Target affinity, off-target binding, and B_{max} values can be determined in binding assays and have to be evaluated in respect to B_{max} over K_D and their according theoretical, observed binding ratios of the target to another off-target ($tBR_{target/off\text{-}target}$).[45] Values more than 5 are considered suitable in these calculations.[45] For **15**, these values are of concern for the $tBR_{5\text{-}HT_7R/\sigma\text{-}receptors}$ even in high 5-HT$_7$R density areas. This is because **15** displays a specific σ-receptor binding component (Figure 2) and σ-receptors are 5-fold more prevalent than the 5-HT$_7$Rs in the highest binding region (thalamus).[6−9,47] Therefore, a specific σ-receptor block may be needed to enable selective 5-HT$_7$R imaging with [^{18}F]**15**. Keeping that in mind, we started to evaluate [^{18}F]**15** in PET experiments.

At first, in vivo evaluation in rats was performed at baseline conditions (Figure 3a,e,f); however, only low brain uptake was observed. Syvänen et al. showed in 2009 that in rodents several well-established PET tracers are *P*-glycoprotein (*P*-gp) efflux transporter substrates. Although these tracers showed poor brain uptake by the rat brain, they have sufficient brain uptake in higher species.[48] Motivated by this, we investigated whether [^{18}F]**15** is also a *P*-gp transporter substrate to potentially explain the low brain uptake. Inhibition of the *P*-gp efflux transporter with elacridar[49] led to increased brain uptake (Figure 3b,e,f), and thus [^{18}F]**15** was confirmed to be a *P*-gp efflux transporter substrate in rats. Next, we tested whether the uptake of [^{18}F]**15** in the brain after *P*-gp inhibition represented specific binding to the 5-HT$_7$R. Brain distribution of [^{18}F]**15** was imaged in rats that were injected with elacridar and a specific 5-HT$_7$R antagonist: the highly 5-HT$_7$R-selective SB-269970[31] or the structurally different antagonist Cimbi-717.[9] Thalamus (tha) and cerebellum (cb) were chosen as the brain regions of interest due to the high abundance of 5-HT$_7$R in thalamus and the low abundance in cerebellum.[6−9] We found that both compounds reduced the area under the time-activity curves (TACs) (SB-269970: tha = 21.6%, cb = 25.5%; Cimbi-717: tha = 38.5%, cb = 35.9%) (Figure 3c–g). The reduction in the thalamus was expected since this is a high 5-HT$_7$R density region. However, the reduction in the cerebellum was to a certain degree unexpected since it is a low 5-HT$_7$R density region.[6−9] Off-target binding of [^{18}F]**15** could explain this observation and since [^{18}F]**15** displayed σ-receptor affinity, we investigated whether σ-receptor binding contributed to the observed PET signal. For this purpose, we imaged [^{18}F]**15** distribution in rat brain under *P*-gp inhibition with elacridar and sigma receptor blockade with either the subtype-unselective σ-receptor antagonist haloperidol (1 mg/kg) or the $\sigma - 1$ selective antagonist SA4503 (1.5 mg/kg).[50] We saw a reduction in the area under the time-activity curves in thalamus and cerebellum both with haloperidol (Figure 3f,g, tha = 24.1% and cb = 16.2%) and with SA4503 (Figure 3g, tha = 13.5% and cb = 12.7%). Accordingly, we conclude that in rats the observed PET signal stems from both 5-HT$_7$R and σ-receptor affinities. This could explain the larger reduction in the PET signal seen in thalamus after pretreatment with Cimbi-717 compared to SB-269970 since Cimbi-717 also displays high affinity for the σ-receptors. A biodistribution study was conducted, concluding that the major excretion pathway was through the kidneys in both situations and with the major difference of distribution seen in brain uptake (Table 3). Full time-activity curves can be found in the Supporting Information (Figure S2).

DOI: 10.1021/acsomega.9b00394
ACS Omega 2019, 4, 7344−7353

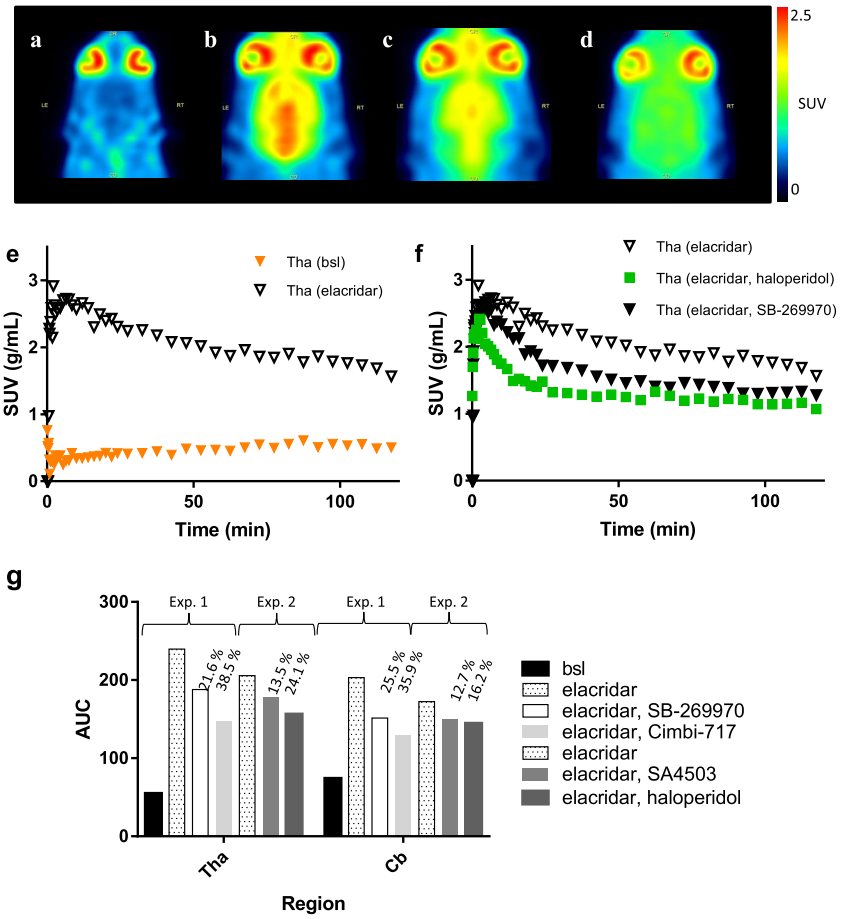

Figure 3. Results from the in vivo evaluation of [^{18}F]**15** in rats. Horizontal PET images of [^{18}F]**15** evaluated in rats (a–d); all summed images are from 5 to 120 min of a dynamic scan obtained in a high-resolution research tomography (HRRT) scanner. (a) Summed PET image of [^{18}F]**15** at baseline. (b) Summed PET image of [^{18}F]**15** after pretreatment with elacridar (5 mg/kg). (c) Summed PET image of [^{18}F]**15** after pretreatment with elacridar (5 mg/kg) and SB-269970 (3 mg/kg). (d) Summed PET image of [^{18}F]**15** after pretreatment with elacridar (5 mg/kg) and Cimbi-717 (3 mg/kg). Time-activity curves (TACs) from PET evaluation of [^{18}F]**15** in rats (e, f). (e) Thalamus (Tha) TACs [^{18}F]**15** in the baseline condition, after pretreatment with elacridar (5 mg/kg). (f) Thalamus (Tha) TACs of [^{18}F]**15** after pretreatment with elacridar (5 mg/kg), both elacridar (5 mg/kg) and SB-269970 (3 mg/kg) and elacridar (5 mg/kg) and haloperidol (1 mg/kg). (g) Calculated area under the curve (AUC) for all TACs displayed as a grouped barplot also indicating percentage AUC reduction above the blocking agent bars. All TACs are normalized to injected radioactivity and animal weight to generate the standard uptake value (SUV). Used dose for SA4503 experiments was 1.5 mg/kg.

Table 3. Biodistribution of [^{18}F]ENL30 in Female Long-Evans Rats (% ID/mL)[a]

organ	5 min	20 min	40 min	60 min	120 min
liver	0.72 ± 0.15	0.43 ± 0.07	0.39 ± 0.05	0.36 ± 0.04	0.39 ± 0.03
kidneys	1.76 ± 0.17	1.24 ± 0.15	1.04 ± 0.15	0.96 ± 0.15	0.82 ± 0.15
bladder	0.49 ± 0.14	1.43 ± 0.48	1.89 ± 0.06	1.81 ± 0.22	2.00 ± 0.45
brain (baseline)	0.21 ± 0.02	0.21 ± 0.02	0.22 ± 0.02	0.23 ± 0.02	0.26 ± 0.02
brain (elacridar)	0.90 ± 0.31	0.78 ± 0.29	0.68 ± 0.25	0.62 ± 0.21	0.56 ± 0.16

[a]Data are presented as the mean ± standard deviation of four animals at 5, 20, 40, 60, and 120 min after intravenous injection of [^{18}F]ENL30.

CONCLUSIONS

[^{18}F]ENL30 ([^{18}F]**15**) was successfully synthesized using a convergent synthesis method. In rat brain slices in vitro, [^{18}F]**15** showed low nanomolar affinity toward 5-HT$_7$R (K_D = 0.75 nM). In vivo [^{18}F]**15** displayed specific binding to 5-HT$_7$R but also to σ-receptors. To which extent this will translate into higher species will need to be determined, but it is likely that the *P*-gp dependency of [^{18}F]**15** will present less of a problem.[48] Even if the in vivo PET signal of [^{18}F]**15** also turns out to represent specific binding to σ-receptors in higher species, specific blocking of σ-receptors could potentially enable PET imaging of the 5-HT$_7$R system.

EXPERIMENTAL SECTION

General Information. Solvents and reagents were purchased from Sigma-Aldrich (Merck, Darmstadt, Germany) or Thermo Fisher Scientific and used as received unless otherwise noted. The precursors for the radiosynthesis, ethylene di(*p*-toluenesulfonate) (Merck, Darmstadt, Germany) and SB-269970 (Tocris Bioscience, Abingdon, U.K.), were commercially available.

DOI: 10.1021/acsomega.9b00394
ACS Omega 2019, 4, 7344–7353

NMR (^{1}H, ^{13}C) spectra were recorded on a 600 MHz Bruker Avance III HD or a 400 MHz Bruker Avance II at room temperature. Chemical shift (δ) is expressed in parts per million and referenced to the residual solvent peak. The resonance multiplicity is abbreviated as follows or combinations thereof: s (singlet), d (doublet), t (triplet), p (quintet), and m (multiplet). The analysis of the NMR spectra was performed using the software MestReNova v12.0.0 (Mestrelab Research S.L.). Thin-layer chromatography (TLC) was run on silica-plated aluminum sheets (Silica gel 60 F254) from Merck. The spots were visualized by ultraviolet light at 254 nm, and the fraction of radioactivity on the TLC plates was measured with an instant imager from Packard. Flash column chromatography was carried out manually on silica gel 60 (0.040−0.063 mm). Analytical high-performance liquid chromatography (HPLC) was performed on a Dionex system consisting of a P680A pump, a UVD 170U detector, and a Scansys radiodetector. The HPLC system was controlled by Chromeleon 6.8 software.

*Synthesis of ENL30 (**15**).* The reference compound ENL30 ((*R*)-1-(2-(1-((3-(2-fluoroethoxy)phenyl)sulfonyl)pyrrolidin-2-yl)ethyl)-4-methylpiperidine) (**15**) was synthesized by a multistep reaction with the final step being the deprotection of *tert*-butyl-(*R*)-2-(2-(4-methylpiperidin-1-yl)ethyl)pyrrolidine-1-carboxylate (**8**) to (*R*)-4-methyl-1-(2-(pyrrolidin-2-yl)ethyl)-piperidine (**9**) and subsequent coupling with its sulfonyl chloride coupling partner 3-(2-fluoroethoxy)benzenesulfonyl chloride (**13**). (**8**) was synthesized by optimization of previous protocols;[31,35,36] see the Supporting Information. The synthesis of (**13**) and the final reaction step are described below.

*3-(Benzylthio)phenol (**12**).* Benzyl bromide (0.52 mL, 4.4 mmol) was added to a solution of 3-mercaptophenol (0.4 mL, 3.96 mmol) and sodium hydroxide (175.9 mg, 4.4 mmol) in methanol (10 mL). The mixture was stirred overnight at room temperature and was then diluted with water (20 mL) and acetic acid (10 mL). The resultant mixture was then concentrated to remove organic solvents. Also, the resultant precipitate was collected by filtration and washed with water to yield the pure product (558.1 mg, 58.6%). ^{1}H NMR (400 MHz, methanol-d_4) δ 7.35−7.20 (m, 5H), 7.09 (t, J = 7.7 Hz, 1H), 6.82−6.77 (m, 2H), 6.63 (ddd, J = 8.1, 2.3, 1.0 Hz, 1H), 4.14 (s, 2H). Figure S21. R_f = 0.78 (7:3 Hept/EtOAc).

*Benzyl(3-(2-fluoroethoxy)phenyl)sulfane (**13**).* To a solution of sodium hydride (61.89 mg, 2.58 mmol) in anhydrous DMF (10 mL) under a nitrogen atmosphere was added a solution of **12** (558.1 mg, 2.58 mmol) in anhydrous DMF (7 mL) under cooling at 0 °C. The solution was allowed to stir for 30 min, after which, with the solution still at 0 °C, 1-bromo-2-fluoroethane (0.2 mL, 2.58 mmol) was slowly added. The mixture was stirred for a further 20 h at 60 °C. Then, the solvent was removed in vacuo. The residue was then redissolved in ethyl acetate, washed with water and brine, dried over $MgSO_4$, and concentrated. The crude product was then purified by flash chromatography (125.4 mg, 18.6%). ^{1}H NMR (400 MHz, methanol-d_4) δ 7.36−7.22 (m, 5H), 7.19 (t, J = 8.0 Hz, 1H), 6.94 (ddd, J = 7.8, 1.8, 0.9 Hz, 1H), 6.89 (dd, J = 2.5, 1.7 Hz, 1H), 6.79 (ddd, J = 8.3, 2.5, 0.9 Hz, 1H), 4.78−4.73 (m, 1H), 4.66−4.61 (m, 1H), 4.20−4.17 (m, 1H), 4.16 (s, 2H), 4.13−4.10 (m, 1H). Figure S22. R_f = 0.51 (7:3 Hept/EtOAc).

*3-(2-Fluoroethoxy)benzenesulfonyl Chloride (**14**).* To an ice-cold solution of **13** (125.4 mg, 0.36 mmol) in a mixture of acetonitrile (3.6 mL), water (0.1 mL), and acetic acid (0.15 mL), 2,4-dichloro-5,5-dimethylhydontoin (141.8 mg, 0.72 mmol) was added portion wise. The reaction mixture was stirred at 0 °C while monitoring the consumption of starting material by TLC. Upon consumption of the starting material, the solution was concentrated to near dryness in vacuo. The crude product was then diluted with DCM (4.5 mL), and the solution was cooled once more to 0 °C. The solution was then diluted further with an aqueous 5% $NaHCO_3$ solution. The mixture was stirred for a further 15 min. The lower organic layer was then washed with an aqueous 10% brine solution, and the resultant organic layer was dried over $MgSO_4$ and concentrated in vacuo to give an acceptably pure product (85.9 mg, 100%). ^{1}H NMR (600 MHz, chloroform-*d*) δ 7.68−7.65 (m, 1H), 7.55−7.52 (m, 2H), 7.31 (dt, J = 8.3, 1.6 Hz, 1H), 4.85−4.82 (m, 1H), 4.77−4.74 (m, 1H), 4.35−4.31 (m, 1H), 4.31−4.27 (m, 1H). ^{13}C NMR (151 MHz, chloroform-*d*) δ 158.87, 145.23, 130.75, 122.41, 119.68, 111.85, 81.91, 80.77. Figures S23 and S24. R_f = 0.43 (7:3 Hept/EtOAc).

*(R)-1-(2-(1-((3-(2-Fluoroethoxy)phenyl)sulfonyl)pyrrolidin-2-yl)ethyl)-4-methylpiperidine (ENL30) (**15**).* **9** (4.5 mg, 15.2 μmol) was dissolved in a 1:2 solution of TFA and DCM (1.5 mL), and the resulting solution was stirred under nitrogen for 30 min. The organics were then removed in vacuo, and the residual salt was dissolved in 5 mL of 2 M NaOH at 0 °C. To the aqueous solution was added **14** (13.7 mg, 41.9 μmol) in diethyl ether (4 mL) while still at 0 °C. The resultant biphasic solution was stirred vigorously overnight while warming to room temperature. The reaction mixture was diluted with DCM and acidified to pH 5. The organic layers were washed with water (2 × 5 mL) and then saturated aqueous Na_2HCO_3 (3 × 5 mL). Subsequently, they were dried and concentrated under reduced pressure. The product was of sufficient purity to be used as an HPLC standard for subsequent labeling studies (6 mg, 15 μmol, 99%). ^{1}H NMR (600 MHz, chloroform-*d*) δ 7.45−7.43 (m, 2H), 7.37−7.36 (m, 1H), 7.15 (td, J = 4.5, 2.6 Hz, 1H), 4.84−4.81 (m, 1H), 4.74 (dd, J = 4.7, 3.5 Hz, 1H), 4.30 (td, J = 3.5, 1.2 Hz, 1H), 4.27−4.24 (m, 1H), 3.73 (p, J = 6.7 Hz, 1H), 3.40 (ddd, J = 10.5, 7.2, 4.7 Hz, 1H), 3.19 (dt, J = 10.5, 7.3 Hz, 1H), 3.15−2.98 (m, 2H), 2.26−2.18 (m, 1H), 2.12−1.98 (m, 2H), 1.84−1.48 (m, 5H), 1.46−1.18 (m, 6H), 0.95 (d, J = 6.2 Hz, 3H). ^{13}C NMR (151 MHz, chloroform-*d*) δ 158.90, 130.42, 128.89, 128.03, 120.44, 119.64, 113.26, 82.40, 81.26, 77.37, 67.65, 49.09, 43.96, 31.09, 29.85, 24.19, 14.27. Figures S25 and S26. HPLC [Luna, 5μ, C-18(2) 100 Å column (Phenomenex Inc. 150 × 4.6 mm^2)]; 0.1% TFA in acetonitrile/water (0−100%) over 15 min; 2 mL/min−rt = 6.7 min.

Radiochemistry. *Production of Fluoride-18.* [^{18}F]Fluoride was produced via the (p,n)-reaction in a cyclotron (CTI Siemens and Scanditronix, Rigshospitalet, Denmark) by irradiating [^{18}O]H_2O with a 11 MeV proton beam.

*Radiosynthesis of [^{18}F]ENL30 ([^{18}F]**15**).* The radiosynthesis of [^{18}F]**15** was performed in two steps on a fully automated system (Scansys Laboratorieteknik synthesis module), beginning with the production of the synthon [^{18}F]fluoroethyl tosylate ([^{18}F]FETos), which thereafter was used to [^{18}F]fluoroalkylate the commercially available precursor SB-269970, as shown in Scheme 1.

No-carrier-added aqueous ^{18}F-fluoride from the target was collected at a nonconditioned, activated (10 mL ethanol, 20 mL water, and dried with air) QMA anion-exchange cartridge (Sep-Pak Accell Plus QMA Plus Light, chloride form, Waters). A solution of 20 mg of 1,10-diaza-4,7,13,16,21,24-hexaoxabicyclo[8.8.8]hexacosane (Kryptofix-222) and 3.3 mg of K_2CO_3 in 0.65 mL of 97% aqueous methanol was used to elute the [^{18}F]fluoride off the cartridge. The elute was thereafter

DOI: 10.1021/acsomega.9b00394
ACS Omega 2019, 4, 7344−7353

dried by evaporation at first 110 °C under nitrogen and then dried twice again with 1 mL of acetonitrile; during the last step, the temperature was lowered to 80 °C. To the dried Kryptofix-222/[^{18}F]fluoride complex, 4 mg (0.011 mmol) of the precursor ethylene di(*p*-toluenesulfonate), dissolved in 1 mL of MeCN, was added, and the mixture was further heated for 3 min.

[^{18}F]FETos was isolated using semipreparative HPLC [Luna 5 μm C-18(2) 100 Å column (Phenomenex Inc. 250 × 10 mm^2), H_2O/MeCN (40:60), at a flow rate of 6 mL/min]. The retention times were 330 s for [^{18}F]FETos and 150 s for ethylene di(*p*-toluenesulfonate). The HPLC fraction containing the [^{18}F]FETos was thereafter diluted with water (60 mL), and the product was loaded on a Sep-Pak C-18 Plus Short Cartridge, Waters. The cartridge was dried with nitrogen before the [^{18}F]FETos was eluted off with 1 mL of DMSO into a vial containing 3 mg of SB-269970 (0.008 mmol) and 5 μL of NaOH 2N, dissolved in 300 μL of DMSO and preheated at 100 °C since the start of synthesis (40 min). The reaction mixture was further heated at 100 °C for 25 min before the final isolation of [^{18}F]**15**, using semipreparative HPLC [Luna 5 μm C-18(2) 100 Å column (Phenomenex Inc. 250 × 10 mm^2), EtOH/0.1% phosphoric acid in water (25:75), at a flow rate of 3 mL/min]. The final product had a retention time of 1200 s and was collected in a sterile 20 mL vial and diluted with phosphate-buffer (4 mL, 100 mM, and pH 7). The retention times of [^{18}F]FETos and SB-269970 were 300−400 and 550 s, respectively.

Determination of Radiochemical Purity and Molar Activity. The preparation of the final product was visually inspected for clarity and absence of color and particles. Chemical and radiochemical purities were evaluated by analytical HPLC [Luna, 5μ, C-18(2) 100 Å column (Phenomenex Inc. 150 × 4.6 mm^2); 0.1% TFA in acetonitrile/water (0−100%) over 15 min; 2 mL/min; retention times for [^{18}F]FETos = 7.4 min, [^{18}F]**15** = 6.7 min, SB-269970 = 5 min, and [^{18}F]F$^-$ = 1−2 min]. TLC analyses were also carried out to see the final content of [^{18}F]fluoride (SiO_2-TLC: eluent: EtOAc, R_f [^{18}F]**15**: 0.25 and R_f [^{18}F]fluoride ion: 0.0). The total synthesis time was 2.5 h, and the product could be produced with molar activities between 108 and 197 GBq/μmol (n = 3) and radiochemical purities above 98%.

Animals. All procedures were conducted in accordance with the FELASA guidelines for animal research and with approval from The Danish Animal Experiments Inspectorate (license number: 2017-15-0201-01283) as well as the Department of Experimental Medicine, University of Copenhagen. In both the in vitro and in vivo studies, we used 200−250 g female Long-Evans WT rats, which were housed in groups of 2−4 animals per cage in a climate-controlled rodent facility with a 12 h dark/12 h light cycle. For the PET experiments, the rats were transported to the scanner at least 1 h before starting the experiment and they were all fed ad libitum and had free access to water.

In Vitro [^{18}F]15 Autoradiography. After decapitation of three female Long-Evans WT rats, the brains were quickly removed, rinsed in ice-cold water, and frozen using dry ice. After storage at −80 °C, the brains were cut with a cryostat (Microme HM 500 OM) and 20 μm coronal sections were collected on glass slides (Thermo Scientific Superfrost Plus), starting at bregma −1.8 mm to around −4 mm to get slices containing thalamus. The brain sections were stored at −80 °C until the day of the experiment.

In Vitro Autoradiography for K_D and B_{max} Determination. On the day of the experiment, the sections were thawed for 1−2 h prior to the start and thereafter preincubated for 30−60 min in assay buffer (Tris−HCl 50 mM, pH 7.4, rt). The sections were then incubated for 60 min at room temperate in assay buffer modified by the addition of [^{18}F]**15** to the final concentrations of 0.1, 0.3, 0.7, 1, and 2 nM. For every second section, SB-269970 (10 μm) was added to both the preincubation and incubation buffer to determine the non-specific binding. The incubation was thereafter terminated by washing two times for 5 min in ice-cold assay buffer. The sections were quickly rinsed in ice-cold water for 20 s and then rapidly dried under a gentle stream of air before exposure to an imaging plate (BAS-MS 2040, Fujifilm) overnight.

After obtaining the images using the BAS-1800 plate reader (Fujifilm), ImageJ v1.52i was used for image analysis and GraphPad Prism 7 for calculations and statistics. K_D and B_{max} were determined in the thalamus, by calculating the specific binding (SB) by subtraction of the nonspecific binding from the total binding, after drawing a region of interest containing thalamus on all brain slices (as defined in Figure 1). A calibration curve of [^{18}F]**15** solutions applied on a TLC plate and exposed together with the slices was used to recalculate the intensity into concentrations in nanomolar. A one-sited (specific binding) nonlinear regression was used to acquire the K_D and B_{max} values.

In Vitro Autoradiography: Blocking Study. On the day of the experiment, the sections were thawed for 1−2 h prior to start and thereafter preincubated for 30−60 min in assay buffer (Tris−HCl 50 mM, pH 7.4, rt). The sections were then incubated for 60 min at room temperate in assay buffer modified by the addition of [^{18}F]**15** to the final concentration of 5 nM. Either SB-269970 (1, 10, 50, or 100 nM), Haloperidol (1, 10, 50, or 100 nM, Janssen-Cilag, Birkerød, Denmark), or SA4503 (1, 10, 50, or 100 nM, Merck, Darmstadt, Germany) was added to both the preincubation and incubation buffer to determine whether a dose-dependent blocking effect could be seen in thalamus. The incubation was thereafter terminated by washing two times for 5 min in ice-cold assay buffer. The sections were quickly rinsed in ice-cold water for 20 s and then rapidly dried under a gentle stream of air before being exposed to an imaging plate (BAS-MS 2040, Fujifilm) for 60 min. After obtaining the images using the BAS-1800, ImageJ v1.52i was used for image analysis and GraphPad Prism 7 for the statistical calculations and presentation.

PET Evaluation in Rats. Anesthesia was induced at 3−3.5% isoflurane in oxygen and maintained at 2−2.5% during scans. The PET tracers were given as intravenous (iv) bolus injections in tail vein catheters at the start of the scan, with the injected doses being between 15 and 25 MBq. The rats were subsequently scanned in a high-resolution research tomography (HRRT) scanner (Siemens AG, Munich, Germany), first for a 120 min dynamic PET scan followed by a point source transmission scan. The scans were performed using a homemade 2 × 2 rat insert, which enabled the possibility of scanning four rats simultaneously.[51] The animals were scanned at baseline and after receiving iv pretreatment of either elacridar[49] (5 mg/kg, Carbosynth, Compton, U.K.) and/or either SB-269970 (3 mg/kg), Cimbi-717 (3 mg/kg, synthesized in house),[9] haloperidol (1 mg/kg), or SA4503 (1.5 mg/kg) 15−30 min before tracer injection. SB-269970, Cimbi-717, and SA4503 were initially dissolved in DMSO and then added to a 10% β-cyclodextrin solution (Merck, Darmstadt, Germany). Haloperidol was diluted to the desired concentration with sterile water.

Reconstruction and Processing of PET Data. The 120 min list-mode PET data was reconstructed using the three-

DOI: 10.1021/acsomega.9b00394
ACS Omega 2019, 4, 7344−7353

dimensional-ordered subset expectation maximization algorithm with attenuation and scatter correction, into 45 dynamic frames (6 × 10, 6 × 20, 6 × 60, 8 × 120, and 19 × 300 s), and the images consisted of 207 planes of 256 × 256 voxels of 1.22 × 1.22 × 1.22 mm^3. Using Pmod, an averaged picture of all frames, except for the first 5 min, were reconstructed for each rat and used for co-registration to a standardized MRI-based rat brain atlas (Swartz). Volumes of interest (VOIs) containing thalamus and cerebellum were extracted from the VOI template defined for the MRI-based atlas.[52,53] The outcome measure in the time-activity curves (TACs) was calculated as radioactive concentration in VOI (kBq/cc) normalized to the injected dose and corrected for the weight of the animal yielding standardized uptake values (SUV). GraphPad Prism 7 was used for calculating the AUC for all TACs and displaying the results as a grouped barplot. For the biodistribution study, VOIs were manually drawn containing the organs of intrest and visualized as TACs with the unit ID%/mL.

■ ASSOCIATED CONTENT

Supporting Information

The Supporting Information is available free of charge on the ACS Publications website at DOI: 10.1021/acsomega.9b00394.

Compounds **10**−**15** (CSV)

HPLC chromatograms and NMR spectra; summary of the B_{max} of 5-HT_7R in different species and brain regions; attempted catalytic coupling; time-activity curves (TACs) from PET evaluation of [^{18}F]ENL30 in rats; synthetic overview of the synthesis of *tert*-butyl-(*R*)-2-(2-(4-methylpiperidin-1-yl)ethyl)pyrrolidine-1-carboxylate (**9**); semipreparative HPLC chromatograms for isolation of [^{18}F]FETos; analytical HPLC radio chromatogram of the crude reaction mixture; semipreparative HPLC chromatograms for isolation of the final product [^{18}F]-ENL30; analytical HPLC radio and UV chromatogram of the isolated product [^{18}F]ENL30 and the reference compound ENL30; results of the in vitro autoradiography of [^{18}F]**15** (PDF)

■ AUTHOR INFORMATION

Corresponding Author

*E-mail: matthias.herth@sund.ku.dk. Tel.: +45 93565414. Fax: +45 35 33 60 41.

ORCID

Elina Tampio L'Estrade: 0000-0003-4368-4660

Matthias M. Herth: 0000-0002-7788-513X

Author Contributions

Experimental work and data evaluation were carried out by E.T.L., F.G.E., M.X., S.L.B., M.E., and M.P. V.S., T.G.O., G.M.K., and M.M.H. designed the experiments, supervised the work, contributed to the research idea, and were strongly involved in the evaluation of the experimental data. The manuscript was written through contributions of all authors. All authors have given approval to the final version of the manuscript.

Notes

The authors declare no competing financial interest.

■ ACKNOWLEDGMENTS

The authors wish to thank the staff at the PET and Cyclotron unit at Rigshospitalet, Copenhagen, Denmark, for expert technical assistance.

■ REFERENCES

(1) Matthys, A.; Haegeman, G.; Van Craenenbroeck, K.; Vanhoenacker, P. Role of the 5-HT_7 receptor in the central nervous system: from current status to future perspectives. *Mol. Neurobiol.* **2011**, *43*, 228−253.

(2) Nichols, D. E.; Nichols, C. D. Serotonin Receptors. *Chem. Rev.* **2008**, *108*, 1614−1641.

(3) Bard, J. A.; Zgombick, J.; Adham, N.; Vaysse, P.; Branchek, T. A.; Weinshank, R. L. Cloning of a novel human serotonin receptor (5-HT7) positively linked to adenylate cyclase. *J. Biol. Chem.* **1993**, *268*, 23422−23426.

(4) Lovenberg, T. W.; Baron, B. M.; de Lecea, L.; Miller, J. D.; Prosser, R. A.; Rea, M. A.; Foye, P. E.; Racke, M.; Slone, A. L.; Siegel, B. W.; et al. A novel adenylyl cyclase-activating serotonin receptor (5-HT7) implicated in the regulation of mammalian circadian rhythms. *Neuron* **1993**, *11*, 449−458.

(5) Ruat, M.; Traiffort, E.; Leurs, R.; Tardivel-Lacombe, J.; Diaz, J.; Arrang, J.-M.; Schwartz, J.-C. Molecular cloning, characterization, and localization of a high-affinity serotonin receptor (5-HT7) activating cAMP formation. *Proc. Natl. Acad. Sci. U.S.A.* **1993**, *90*, 8547−8551.

(6) Gustafson, E. L.; Durkin, M. M.; Bard, J. A.; Zgombick, J.; Branchek, T. A. A receptor autoradiographic and in situ hybridization analysis of the distribution of the 5-ht7 receptor in rat brain. *Br. J. Pharmacol.* **1996**, *117*, 657−666.

(7) Varnäs, K.; Thomas, D. R.; Tupala, E.; Tiihonen, J.; Hall, H. Distribution of 5-HT7 receptors in the human brain: a preliminary autoradiographic study using [3H] SB-269970. *Neurosci. Lett.* **2004**, *367*, 313−316.

(8) Horisawa, T.; Ishiyama, T.; Ono, M.; Ishibashi, T.; Taiji, M. Binding of lurasidone, a novel antipsychotic, to rat 5-HT7 receptor: analysis by [3H] SB-269970 autoradiography. *Prog. Neuro-Psychopharmacol. Biol. Psychiatry* **2013**, *40*, 132−137.

(9) Hansen, H. D.; Herth, M. M.; Ettrup, A.; Andersen, V. L.; Lehel, S.; Dyssegaard, A.; Kristensen, J. L.; Knudsen, G. M. Radiosynthesis and in vivo evaluation of novel radioligands for PET imaging of cerebral 5-HT7 receptors. *J. Nucl. Med.* **2014**, *55*, 640−646.

(10) Hansen, H. D.; Constantinescu, C. C.; Barret, O.; Herth, M. M.; Magnussen, J. H.; Lehel, S.; Dyssegaard, A.; Colomb, J.; Billard, T.; Zimmer, L. Evaluation of [18F] 2FP3 in pigs and non-human primates. *J. Labelled Compd. Radiopharm.* **2019**, *62*, 34−42.

(11) Guscott, M.; Bristow, L.; Hadingham, K.; Rosahl, T.; Beer, M.; Stanton, J.; Bromidge, F.; Owens, A.; Huscroft, I.; Myers, J. Genetic knockout and pharmacological blockade studies of the 5-HT7 receptor suggest therapeutic potential in depression. *Neuropharmacology* **2005**, *48*, 492−502.

(12) Hedlund, P. B.; Huitron-Resendiz, S.; Henriksen, S. J.; Sutcliffe, J. G. 5-HT7 Receptor Inhibition and Inactivation Induce Antidepressant-like Behavior and Sleep Pattern. *Biol. Psychiatry* **2005**, *58*, 831−837.

(13) Wesołowska, A.; Nikiforuk, A.; Stachowicz, K.; Tatarczyńska, E. Effect of the selective 5-HT7 receptor antagonist SB 269970 in animal models of anxiety and depression. *Neuropharmacology* **2006**, *51*, 578−586.

(14) Wesołowska, A.; Nikiforuk, A.; Stachowicz, K. Potential anxiolytic and antidepressant effects of the selective 5-HT7 receptor antagonist SB 269970 after intrahippocampal administration to rats. *Eur. J. Pharmacol.* **2006**, *553*, 185−190.

(15) Mnie-Filali, O.; Lambas-Señas, L.; Scarna, H.; Haddjeri, N. Therapeutic potential of 5-HT7 receptors in mood disorders. *Curr. Drug Targets* **2009**, *10*, 1109−1117.

(16) Mnie-Filali, O.; Lambás-Señas, L.; Zimmer, L.; Haddjeri, N. 5-HT7 receptor antagonists as a new class of antidepressants. *Drug News Perspect.* **2007**, *20*, 613−618.

DOI: 10.1021/acsomega.9b00394
ACS Omega 2019, 4, 7344−7353

(17) Zimmer, L.; Billard, T. Molecular imaging of the serotonin 5-HT7 receptors: from autoradiography to positron emission tomography. *Rev. Neurosci.* **2014**, *25*, 357−365.
(18) Thomas, D. R.; Atkinson, P. J.; Hastie, P. G.; Roberts, J. C.; Middlemiss, D. N.; Price, G. W. [3H]-SB-269970 radiolabels 5-HT7 receptors in rodent, pig and primate brain tissues. *Neuropharmacology* **2002**, *42*, 74−81.
(19) Paterson, L. M.; Tyacke, R. J.; Nutt, D. J.; Knudsen, G. M. Measuring endogenous 5-HT release by emission tomography: promises and pitfalls. *J. Cereb. Blood Flow Metab.* **2010**, *30*, 1682−1706.
(20) Kristensen, J. L.; Herth, M. M. Textbook of Drug Design and Discovery: In Vivo Imaging in Drug Discovery. In *Textbook of Drug Design and Discovery*; CRC Press, 2017.
(21) Miller, P. W.; Long, N. J.; Vilar, R.; Gee, A. D. Synthesis of 11C, 18F, 15O, and 13N radiolabels for positron emission tomography. *Angew. Chem., Int. Ed.* **2008**, *47*, 8998−9033.
(22) Piel, M.; Vernaleken, I.; Rösch, F. Positron Emission Tomography in CNS Drug Discovery and Drug Monitoring. *J. Med. Chem.* **2014**, *57*, 9232−9258.
(23) Herth, M. M.; Andersen, V. L.; Hansen, H. D.; Stroth, N.; Volk, B.; Lehel, S.; Dyssegaard, A.; Ettrup, A.; Svenningsson, P.; Knudsen, G. M.; Kristensen, J. L. Evaluation of 3-Ethyl-3-(phenylpiperazinylbutyl)-oxindoles as PET Ligands for the Serotonin 5-HT(7) Receptor: Synthesis, Pharmacology, Radiolabeling, and in Vivo Brain Imaging in Pigs. *J. Med. Chem.* **2015**, *58*, 3631−3636.
(24) Lemoine, L.; Andries, J.; Le Bars, D.; Billard, T.; Zimmer, L. Comparison of 4 radiolabeled antagonists for serotonin 5-HT(7) receptor neuroimaging: toward the first PET radiotracer. *J. Nucl. Med.* **2011**, *52*, 1811−1818.
(25) Andriès, J.; Lemoine, L.; Mouchel-Blaisot, A.; Tang, S.; Verdurand, M.; Le Bars, D.; Zimmer, L.; Billard, T. Looking for a 5-HT7 radiotracer for positron emission tomography. *Bioorg. Med. Chem. Lett.* **2010**, *20*, 3730−3733.
(26) Hansen, H. D.; Andersen, V. L.; Lehel, S.; Magnussen, J. H.; Dyssegaard, A.; Stroth, N.; Kristensen, J. L.; Knudsen, G. M.; Herth, M. M. Labeling and preliminary in vivo evaluation of the 5-HT(7) receptor selective agonist [(11)C]E-55888. *Bioorg. Med. Chem. Lett.* **2015**, *25*, 1901−1904.
(27) Lacivita, E.; Niso, M.; Hansen, H. D.; Di Pilato, P.; Herth, M. M.; Lehel, S.; Ettrup, A.; Montenegro, L.; Perrone, R.; Berardi, F.; Colabufo, N. A.; Leopoldo, M.; Knudsen, G. M. Design, synthesis, radiolabeling and in vivo evaluation of potential positron emission tomography (PET) radioligands for brain imaging of the 5-HT(7) receptor. *Bioorg. Med. Chem.* **2014**, *22*, 1736−1750.
(28) Hansen, H. D.; Lacivita, E.; Di Pilato, P.; Herth, M. M.; Lehel, S.; Ettrup, A.; Andersen, V. L.; Dyssegaard, A.; De Giorgio, P.; Perrone, R.; Berardi, F.; Colabufo, N. A.; Niso, M.; Knudsen, G. M.; Leopoldo, M. Synthesis, radiolabeling and in vivo evaluation of [(11)C](R)-1-[4-[2-(4-methoxyphenyl)phenyl]piperazin-1-yl]-3-(2-pyrazinyloxy)-2-p ropanol, a potential PET radioligand for the 5-HT(7) receptor. *Eur. J. Med. Chem.* **2014**, *79*, 152−163.
(29) Colomb, J.; Becker, G.; Forcellini, E.; Meyer, S.; Buisson, L.; Zimmer, L.; Billard, T. Synthesis and pharmacological evaluation of a new series of radiolabeled ligands for 5-HT7 receptor PET neuroimaging. *Nucl. Med. Biol.* **2014**, *41*, 330−337.
(30) Herth, M.; Hansen, H.; Anders, E.; Lehel, S.; Kristensen, J.; Billard, T.; Zimmer, L.; Knudsen, G. Development of a novel 11C-labelled SB-269970 derivative for imaging the cerebral 5-HT7 receptors. *J. Nucl. Med.* **2014**, *55*, No. 1814.
(31) Lovell, P. J.; Bromidge, S. M.; Dabbs, S.; Duckworth, D. M.; Forbes, I. T.; Jennings, A. J.; King, F. D.; Middlemiss, D. N.; Rahman, S. K.; Saunders, D. V.; Collin, L. L.; Hagan, J. J.; Riley, G. J.; Thomas, D. R. A novel, potent, and selective 5-HT(7) antagonist: (R)-3-(2-(2-(4-methylpiperidin-1-yl)ethyl)pyrrolidine-1-sulfonyl) phenol (SB-269970). *J. Med. Chem.* **2000**, *43*, 342−345.
(32) Herth, M. M.; Debus, F.; Piel, M.; Palner, M.; Knudsen, G. M.; Luddens, H.; Rosch, F. Total synthesis and evaluation of [18F]MHMZ. *Bioorg. Med. Chem. Lett.* **2008**, *18*, 1515−1519.
(33) Van Der Born, D.; Pees, A.; Poot, A. J.; Orru, R. V.; Windhorst, A. D.; Vugts, D. J. Fluorine-18 labelled building blocks for PET tracer synthesis. *Chem. Soc. Rev.* **2017**, *46*, 4709−4773.
(34) Kniess, T.; Laube, M.; Brust, P.; Steinbach, J. 2-[18 F] Fluoroethyl tosylate—a versatile tool for building 18 F-based radiotracers for positron emission tomography. *MedChemComm* **2015**, *6*, 1714−1754.
(35) Cardillo, G.; Gentilucci, L.; Qasem, A. R.; Sgarzi, F.; Spampinato, S. Endomorphin-1 analogues containing β-proline are μ-opioid receptor agonists and display enhanced enzymatic hydrolysis resistance. *J. Med. Chem.* **2002**, *45*, 2571−2578.
(36) Chu, W.; Zhang, J.; Zeng, C.; Rothfuss, J.; Tu, Z.; Chu, Y.; Reichert, D. E.; Welch, M. J.; Mach, R. H. N-Benzylisatin Sulfonamide Analogues as Potent Caspase-3 Inhibitors: Synthesis, in Vitro Activity, and Molecular Modeling Studies. *J. Med. Chem.* **2005**, *48*, 7637−7647.
(37) Paryzek, Z.; Koenig, H.; Tabaczka, B. Ammonium formate/palladium on carbon: a versatile system for catalytic hydrogen transfer reductions of carbon-carbon double bonds. *Synthesis* **2003**, *2003*, 2023−2026.
(38) Schjøth-Eskesen, C.; Jensen, H. H. Efficient Arndt−Eistert synthesis of selective 5-HT7 receptor antagonist SB-269970. *Synth. Commun.* **2009**, *39*, 3243−3253.
(39) Nishiguchi, A.; Maeda, K.; Miki, S. Sulfonyl chloride formation from thiol derivatives by N-chlorosuccinimide mediated oxidation. *Synthesis* **2006**, *2006*, 4131−4134.
(40) Veisi, H. Convenient one-pot Synthesis of sulfonamides from thiols and disulfides using 1, 3-dichloro-5, 5-dimethylhydantoin (DCH). *Bull. Korean Chem. Soc.* **2012**, *33*, 383−386.
(41) Ates, A.; Burssens, P.; Lorthioir, O.; Lo Brutto, P.; Dehon, G.; Keyaerts, J.; Coloretti, F.; Lallemand, B.; Verbois, V.; Gillard, M.; et al. 5-HT7 Receptor Antagonists with an Unprecedented Selectivity Profile. *ChemMedChem* **2018**, *13*, 795−802.
(42) McLeod, M. C.; Aubé, J.; Frankowski, K. J. Decahydrobenzoquinolin-5-one sigma receptor ligands: Divergent development of both sigma 1 and sigma 2 receptor selective examples. *Bioorg. Med. Chem. Lett.* **2016**, *26*, 5689−5694.
(43) Li, P.; L Snyder, G.; E Vanover, K. Dopamine targeting drugs for the treatment of schizophrenia: past, present and future. *Curr. Top. Med. Chem.* **2016**, *16*, 3385−3403.
(44) Schotte, A.; Janssen, P.; Gommeren, W.; Luyten, W.; Van Gompel, P.; Lesage, A.; De Loore, K.; Leysen, J. Risperidone compared with new and reference antipsychotic drugs: in vitro and in vivo receptor binding. *Psychopharmacology* **1996**, *124*, 57−73.
(45) Herth, M. M.; Knudsen, G. M. PET Imaging of the 5-HT2A Receptor System: A Tool to Study the Receptor's In Vivo Brain Function. 5-HT2A Receptors in the Central Nervous System. In *5-HT2A Receptors in the Central Nervous System*; Guiard, B., Di, G. G., Eds.; Humana Press: Cham, 2018; Vol. *32*, pp 85−134.
(46) Kessler, R. M.; Ansari, M. S.; de Paulis, T.; Schmidt, D. E.; Clanton, J. A.; Smith, H. E.; Manning, R. G.; Gillespie, D.; Ebert, M. H. High affinity dopamine D2 receptor radioligands. 1. Regional rat brain distribution of iodinated benzamides. *J. Nucl. Med.* **1991**, *32*, 1593−1600.
(47) Weissman, A.; Su, T.-P.; Hedreen, J.; London, E. Sigma receptors in post-mortem human brains. *J. Pharmacol. Exp. Ther.* **1988**, *247*, 29−33.
(48) Syvänen, S.; Lindhe, Ö.; Palner, M.; Kornum, B. R.; Rahman, O.; Långström, B.; Knudsen, G. M.; Hammarlund-Udenaes, M. Species differences in blood-brain barrier transport of three positron emission tomography radioligands with emphasis on *P*-glycoprotein transport. *Drug Metab. Dispos.* **2009**, *37*, 635−643.
(49) Kallem, R.; P Kulkarni, C.; Patel, D.; Thakur, M.; Sinz, M.; P Singh, S.; Shahe Mahammad, S.; Mandlekar, S. A simplified protocol employing elacridar in rodents: a screening model in drug discovery to assess *P*-gp mediated efflux at the blood brain barrier. *Drug Metab. Lett.* **2012**, *6*, 134−144.
(50) Matsuno, K.; Nakazawa, M.; Okamoto, K.; Kawashima, Y.; Mita, S. Binding properties of SA4503, a novel and selective σ1 receptor agonist. *Eur. J. Pharmacol.* **1996**, *306*, 271−279.

DOI: 10.1021/acsomega.9b00394
ACS Omega 2019, 4, 7344−7353

(51) Keller, S. H.; L'Estrade, E. N.; Dall, B.; Palner, M.; Herth, M. In *Quantification Accuracy Of A New Hrrt High Throughput Rat Hotel Using Transmission-based Attenuation Correction: A PHANTOM Study*, Nuclear Science Symposium, Medical Imaging Conference and Room-Temperature Semiconductor Detector Workshop (NSS/MIC/RTSD), 2016; IEEE, 2016; pp 1−3.

(52) Schwarz, A. J.; Danckaert, A.; Reese, T.; Gozzi, A.; Paxinos, G.; Watson, C.; Merlo-Pich, E. V.; Bifone, A. A stereotaxic MRI template set for the rat brain with tissue class distribution maps and co-registered anatomical atlas: application to pharmacological MRI. *Neuroimage* **2006**, *32*, 538−550.

(53) Garcia, D. V.; Casteels, C.; Schwarz, A. J.; Dierckx, R. A.; Koole, M.; Doorduin, J. A standardized method for the construction of tracer specific PET and SPECT rat brain templates: validation and implementation of a toolbox. *PLoS One* **2015**, *10*, No. e0122363.

DOI: 10.1021/acsomega.9b00394
ACS Omega 2019, 4, 7344−7353